JOURNAL OF MATERIALS SCIENCE **39** (2004) 7213–7219

Prediction of macrosegregation during the solidification involving a peritectic transformation for multicomponent steels

L. THUINET, H. COMBEAU
Laboratoire de Science et Génie des Matériaux Métalliques, Ecole des Mines, Parc de Saurupt, 54042 NANCY Cedex, France
E-mail: combeau@mines.inpl-nancy.fr

Micro-macro segregation models are based on the multi-scale approach of the segregation, i.e., on the coupling of a macrosegregation model, which describes transport phenomena at the ingot scale, with a microsegregation model, which describes solidification at the scale of the primary or secondary dendrite arm spacing. The goal of this work is to illustrate the influence of the microsegregation phenomena on the macrosegregation. A microsegregation model for multicomponent steel alloys has been developed which takes into account solutal diffusion in solid and liquid phases, a correct description of the multicomponent phase diagram, and the variation of the local average solute concentration (open system). The peritectic transformation has been tackled and specific attention has been drawn on the accurate determination of the δ/γ and γ/liquid interface movements during solidification. Examples of micro-macro calculations obtained with this microsegregation model on ingot cases are presented and original results which illustrate specific effects of the peritectic transformation on macrosegregation are discussed.

Nomenclature

Latin symbols

w	mass fraction (component) (%wt)
k	partition coefficient
$\bar{w}$	average mass fraction of the calculation domain (component) (%wt)
$\bar{h}$	average specific enthalpy of the domain calculation (J/kg)
f	mass fraction (phase)
g	volume fraction (phase)
h	specific enthalpy (J/kg)
D	diffusion coefficient (m^2/s)
r	spatial variable (m)
T	temperature (°C)
T_{liq}	liquidus temperature (°C)
$m_i^{\varphi 1 \varphi 2}$	local slope of the equilibrium surface $\varphi 1/\varphi 2$ for the solute element i (°C/%wt)
K	permeability (m^2)
k_c	Kozeny constant
t	tortuosity

Greek symbols

φ	phase
δ	ferrite
γ	austenite
λ	characteristic diffusion length (m)
λ_1	primary dendrite arm spacing (m)
λ_2	secondary dendrite arm spacing (m)
ρ	density (kg/m^3)
β_T	thermal expansion coefficient (K^{-1})
β_w^i	solutal expansion coefficient of solute i ($wt\%^{-1}$)
μ	dynamic viscosity (Pa·s)

Superscripts

l	liquid
s	solid
0	initial
$\varphi 1/\varphi 2$	at the $\varphi 1/\varphi 2$ interface, where $\varphi 1, \varphi 2 = \delta, \gamma$ or liquid

Subscripts

i	component

1. Introduction

In an ingot, composition variations in alloy element can be observed at different scales: macrosegregation develops at the scale of the whole product, whereas microsegregation designs the segregation observed at the scale of dendrites. Several fundamental origins of macrosegregation have been identified and recently reviewed [1], among them the liquid flow induced by thermal and solutal gradients which develop during solidification: liquid density is not uniform in the ingot, which causes thermo-solutal convection. A part of these gradients are due to microsegregation, since it induces at the dendrite scale heterogeneities in solute which can

be heavier or lighter than the solvant. Inversely, liquid flow modifies the physical properties of the mushy zone at the micro-scale. So, macrosegregation and microsegregation are strongly coupled. Several works have been already dedicated to microsegregation models applicable for macrosegregation predictions [2–5]. Notably, macrosegregation has been already predicted with microsegregation models coupled with thermodynamic data bases [6, 7]. Among the phase transformations which influence microsegregation, the peritectic transformation has been extensively studied in steels [5, 8–15]: it designs the thickening of a layer of austenite between primary ferrite and liquid on cooling. It is in fact the combination of two kinds of transformation at high temperature: a solid-state $\delta \rightarrow \gamma$ transformation and solidification of austenite. However, even if some microsegregation models coupled with a macrosegregation code [7,16] take into account the peritectic transformation, its eventual specific influence on macrosegregation has not been discussed.

In the present investigation, emphasis is placed on microsegregation, which is mainly determined by the following physical phenomena:

(a) the modification of the average properties of the mushy zone due to the liquid flow, and particularly the variation of the local weight concentration in solute element $i\,\bar{w}_i$,

(b) the solute transport by diffusion in solid and liquid phases,

(c) the phase transformations during solidification: the particular case of the peritectic transformation is studied in this work.

The quantitative prediction of these different phenomena requires an accurate description of the multicomponent phase diagram of the studied alloy (d).

The first part of this work recalls the main assumptions of a previously developed microsegregation model which tackles the problems (a), (b), (c) and (d) and the principle of its coupling with a macrosegregation code. In the second part, examples of results of micro-macro calculations obtained with this microsegregation model are discussed and specific effects of the peritectic transformation on macrosegregation are emphasized.

2. Model description

The different segregation scales in an ingot, as defined above, are represented in Fig. 1. These scales are the bases to understand the mathematical structure of micro-macrosegregation calculations already presented by Combeau *et al*. [17]. It can be divided in two parts: the microscopic and the macroscopic parts. The macroscopic part has been already presented and discussed [18]. It allows the resolution of the averaged continuity equations at the ingot scale, furnishing thus two input values to the micro part: the specific enthalpy $\bar{h}(t)$ and the average solute weight fraction $\bar{w}_i(t)$ for each node of the macroscopic mesh. A control volume of the macroscopic grid is represented in Fig. 1a and b in the mushy zone. From the time variations of $\bar{h}(t)$ and $\bar{w}_i(t)$, a microsegregation model is required to calculate the local solidification path for each node of the macroscopic mesh, i.e., the temperature T, the mass fraction f^{φ} and the profiles of solute weight fraction in each phase φ.

At this stage, one difficulty is to define a suitable representative volume element for the description of microsegregation. The calculation domain for the microsegregation is schematically represented in Fig. 1c. The proposed microsegregation model is 1D. The spatial variable of the domain is noted r and the length of the calculation domain λ. Its choice is very difficult because of the complex morphology of dendrites in the mushy zone. At the microsegregation scale in a columnar zone, several lengths can be chosen as the characteristic microsegregation length: the primary dendrite arm spacing λ_1 [19] or the secondary dendrite arm spacing λ_2 [4]. The discussion of this choice is not in the scope of this paper. In Fig. 1c, the calculation domain of microsegregation has been represented in two

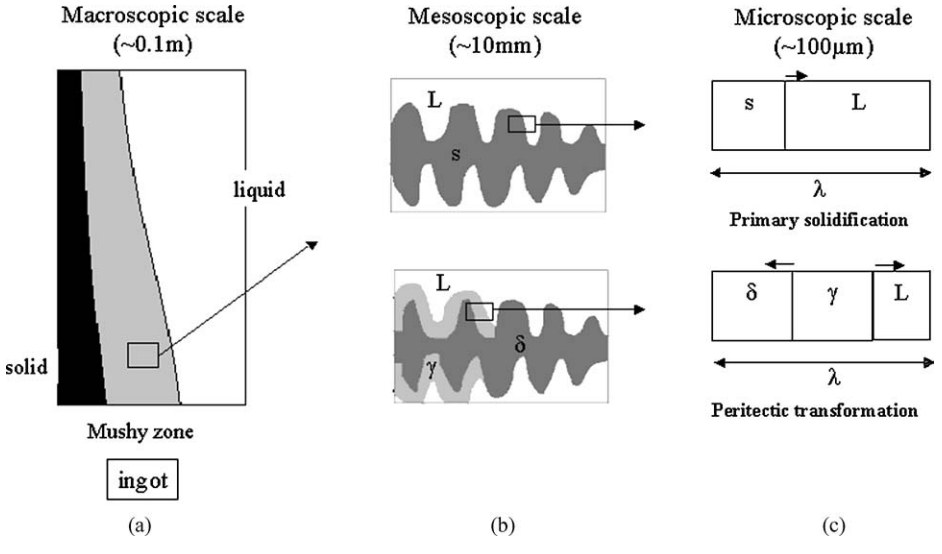

Figure 1 Structure and segregation length scales. The arrows on top of Fig. 1c indicate the movement of the solid/liquid, δ/γ, and γ/liquid interfaces during the primary solidification and the peritectic transformation.

configurations: during primary solidification or during the peritectic transformation.

The main assumptions of the microsegregation model have been already exposed in reference [17] and are recalled below:

1. Temperature T is uniform in the microsegregation calculation domain
2. Densities of the liquid and solid phases are equal and constant
3. Local chemical equilibrium is assumed to be achieved at each interface. This means that the interfacial solute weight fractions in each phase are determined by means of the thermodynamic equilibrium phase diagram.

The microsegregation model is based on the energy balance, which relies the average enthalpy $\bar{h}$ of the domain to the enthalpy h^{φ} of each phase φ through the relation:

$$\bar{h} = \sum_{\varphi} f^{\varphi} h^{\varphi} \tag{1}$$

Furthermore, the only solute transport phenomenon which is considered in the present investigation is diffusion. The diffusion coefficient of solute i in phase φ D_{i}^{φ} is assumed to follow a standard Arrhenius law:

$$D_{\mathrm{i}}^{\varphi} = D_{\mathrm{i}}^{\varphi 0} \exp\left(-\frac{Q_{\mathrm{i}}^{\varphi}}{RT}\right) \tag{2}$$

where $D_{\mathrm{i}}^{\varphi 0}$ is the frequency factor term (m^2/s), Q_{i}^{φ} the molar activation energy (J/mol), R the gas constant ($R = 8.314\ \mathrm{J \cdot mol^{-1} \cdot K^{-1}}$).

Solid-state diffusion is particularly important to describe correctly the peritectic transformation: apart from the well-known analytical equation obtained by Brody-Flemings [20] and modified by Clyne–Kurz [21], more sophisticated numerical models have been tested to handle the problem of solid-state diffusion. These models are based on the approximation of the solute profile in the solid phase by a polynomial [2, 3] or on the Landau transformation [2, 22]. This last method has been adopted, indeed a preliminary study has shown that a polynomial approach is not able to tackle the sharp solute gradients at the δ/γ interface during the peritectic transformation. The Landau transformation is applied to each phase (ferrite, austenite and liquid): the spatial variable of the domain r is transformed into a reduced variable which varies between 0 and 1. The equation to be solved is given in reference [17] (Equation 3).

The microsegregation calculations through the energy conservation Equation 1 and assumption (3) require the determination of thermodynamic quantities. In the present work, only the ferrite/liquid equilibrium, the austenite/liquid equilibrium and the ferrite/austenite equilibrium have to be considered. The model is so coupled with the software of thermodynamic equilibrium calculations Thermo-Calc, according to a generalisation of the tabular approach exposed in references [17, 22].

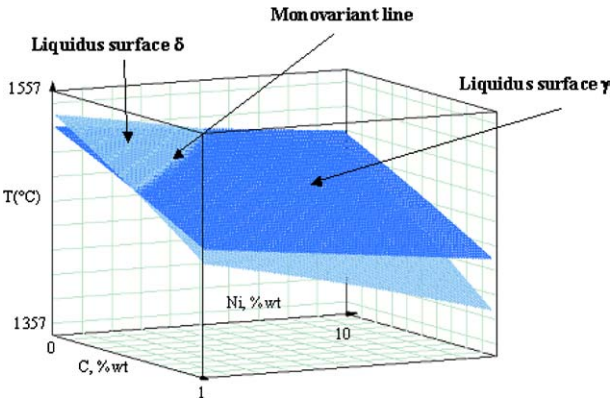

Figure 2 3D representation of δ and γ liquidus surfaces of the Fe-rich corner in the ternary system Fe-Ni-C.

3. Case studies

3.1. Description of the steel ingot simulated

A ternary Fe-Ni-C alloy is considered. The nominal weight fractions are: $w_{\mathrm{C}}^{0} = 0,2$ wt% and $w_{\mathrm{Ni}}^{0} = 2$ wt%. The Fe-Ni-C phase diagram obtained by means of the tabular approach [17, 22] is represented in Fig. 2. It shows that the primary solid phase is ferrite for the chosen nominal weight fractions and the liquidus temperature is 1514°C. The initial temperature of steel is 1540°C: at time $t = 0$, the calculation domain is entirely liquid and the superheat is 26°C. The initial temperature of the mould is 40°C. The simulation domain is shown in Fig. 3. The macroscopic mesh is composed of 3677 control volumes. The geometry of the ingot is axisymmetric. The thermophysical properties of the materials are listed in Table I. A time step of 0.1 s has been used for the computations. The CPU time for a simulation is about 24 h.

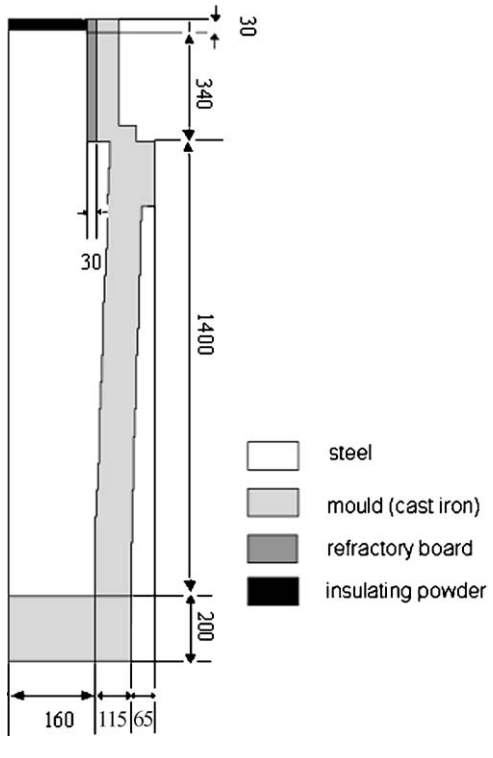

Figure 3 Schematic of the two-dimensional ingot cross section simulated showing all dimensions (in mm) and materials.

TABLE I Thermophysical properties of the cast iron, refractory board, insulating powder and steel

Material	Density (kg/m^3)	Specific heat (J/kg · K)	Thermal conductivity (W/m · K)
Mould (cast iron)	7000	540	26.3
Refractory board	185	1040	1.4
Insulating powder	260	1040	1.88
Solid steel	7060	700	29
Liquid steel	7060	700	39.3

TABLE II Values of the thermophysical properties

β_T	$-8.8527 \cdot 10^{-5}$ K^{-1}
β_w^c	-0.01416% wt^{-1}
β_w^{Ni}	$6.85 \cdot 10^{-4}\%$ wt^{-1}
λ_1	1 mm
Pure iron liquid density	7060 Kg/m^3
μ	0.0042 Pa · s
t	2
k_c	5

TABLE III Diffusion coefficients for Fe-Ni-C alloy used in the model calculations (m^2/s) [23]

	Ferrite	Austenite	Liquid
C	$3.95 \exp(-63\,400/RT) \times 10^{-7}$	$2.55 \exp(-147\,723/RT) \times 10^{-5}$	10^{-9}
Ni	$1.6 \exp(-240\,000/RT) \times 10^{-4}$	$3.5 \exp(-286\,000/RT) \times 10^{-5}$	10^{-9}

In the macrosegregation model, the liquid density and the local permeability are calculated from the following relations:

$$\rho^1\left(T, w_i^1\right) = \rho^0\left[1 - \beta_T(T - T^0) - \sum_i \left(\beta_i^w\left(w_i^1 - w_i^0\right)\right)\right] \quad (3)$$

$$K = \frac{g_1^3 \lambda_1^2}{\pi^2 k_c t^2 (1 - g_1)^2} \quad (4)$$

ρ^0, T^0, w_i^0 are referential values.

The values of the physical quantities which appear in Equations 3 and 4 are given in Table II. The value of λ_1 has been fixed to 1 mm in order to promote the liquid convection during solidification.

The size of the representative microsegregation domain λ has been arbitrarily fixed to 100 μm, i.e., ten times lower than λ_1 and the microscopic geometry is assumed to be cartesian. Diffusion coefficients of carbon and nickel are given in Table III.

3.2. Results and discussion

The macrosegregation patterns in carbon and nickel are represented in Fig. 4 during solidification. The Fig. 4c and f correspond respectively to the final patterns of carbon and nickel after the end of solidification, i.e., after about 6500 s. During solidification, the macrosegregation patterns in carbon (Fig. 4b) and nickel (Fig. 4e) have qualitatively the same aspect:

- a negatively segregated zone in the lower part of the ingot
- a positively segregated zone which develops along the top part of the centerline of the ingot

In order to understand these results, the evolution of the liquid weight fraction in carbon and nickel have been calculated by using independently the microsegregation model. For this calculation, the evolution of the average properties of the microsegregation calculation domain is described by:

$$\frac{\partial \bar{h}}{\partial t} = -700 \text{ W/kg} \quad (5)$$

$$\frac{\partial \bar{w}_i}{\partial t} = 0\% \text{ wt/s (closed system)} \quad (6)$$

For this time variation of $\bar{h}$, the total solidification time is 435 s, which is close to the local solidification time of a point of the ingot located on the centerline, at 150 mm from the bottom part of the mould. In Fig. 5a), the evolution of the carbon weight fraction in liquid is represented in continuous line for this microcalculation: during primary solidification, the liquid is enriched in carbon and nickel ($k_c^{\delta/1} < 1$ and $k_{Ni}^{\delta/1} < 1$), which results in a first transition from primary solidification to peritectic transformation when the solidification path reaches the monovariant line (which is represented in Fig. 2). This first stage of solidification corresponds to the region numbered 1 in Fig. 5a). During the peritectic transformation (region 2 in Fig. 5a), the austenite layer thickens between ferrite and liquid. In this example, the limiting phase of the peritectic transformation is ferrite. The last stage of solidification corresponds to solidification of austenite (region 3 in Fig. 5a), after the complete transformation of ferrite in austenite. For the ingot calculation, these three stages of solidification can be observed in Fig. 4d inside the mushy zone. The evolution of the ferrite fraction is not monotonous: in the first part of the mushy zone in contact with the liquid, this fraction increases during solidification (primary solidification in ferrite) whereas in the second part of the mushy zone, this fraction decreases during solidification (peritectic transformation).

Knowing the solidification path in the absence of macroscopic solute transport, it is possible to deduce the evolution of the liquid density in the mushy zone by using expression (3). The numerical values of Table II and the thermodynamic liquidus slopes $m_i^{s/1}$ calculated by Thermo-Calc shows that $|\beta_w^c + \beta_T m_c^{l/s}| > |\beta_w^{Ni} + \beta_T m_{Ni}^{l/s}|$ during solidification. Consequently, carbon dominates the total buoyancy force in the mushy zone. Furthermore, $|\beta_w^c| > |\beta_T m_c^{l/s}|$, which means that the effect of solutal buoyancy outweighs the effects of thermal buoyancy for carbon. So, during solidification, liquid density decreases, as shown in Fig. 5b), which represents the evolution of the relative liquid density $(\rho^1(T, w_i^1) - \rho^1(T_{liq}, w_i^0))/\rho^1(T_{liq}, w_i^0)$ as a function of the solid fraction. This evolution is coherent with the

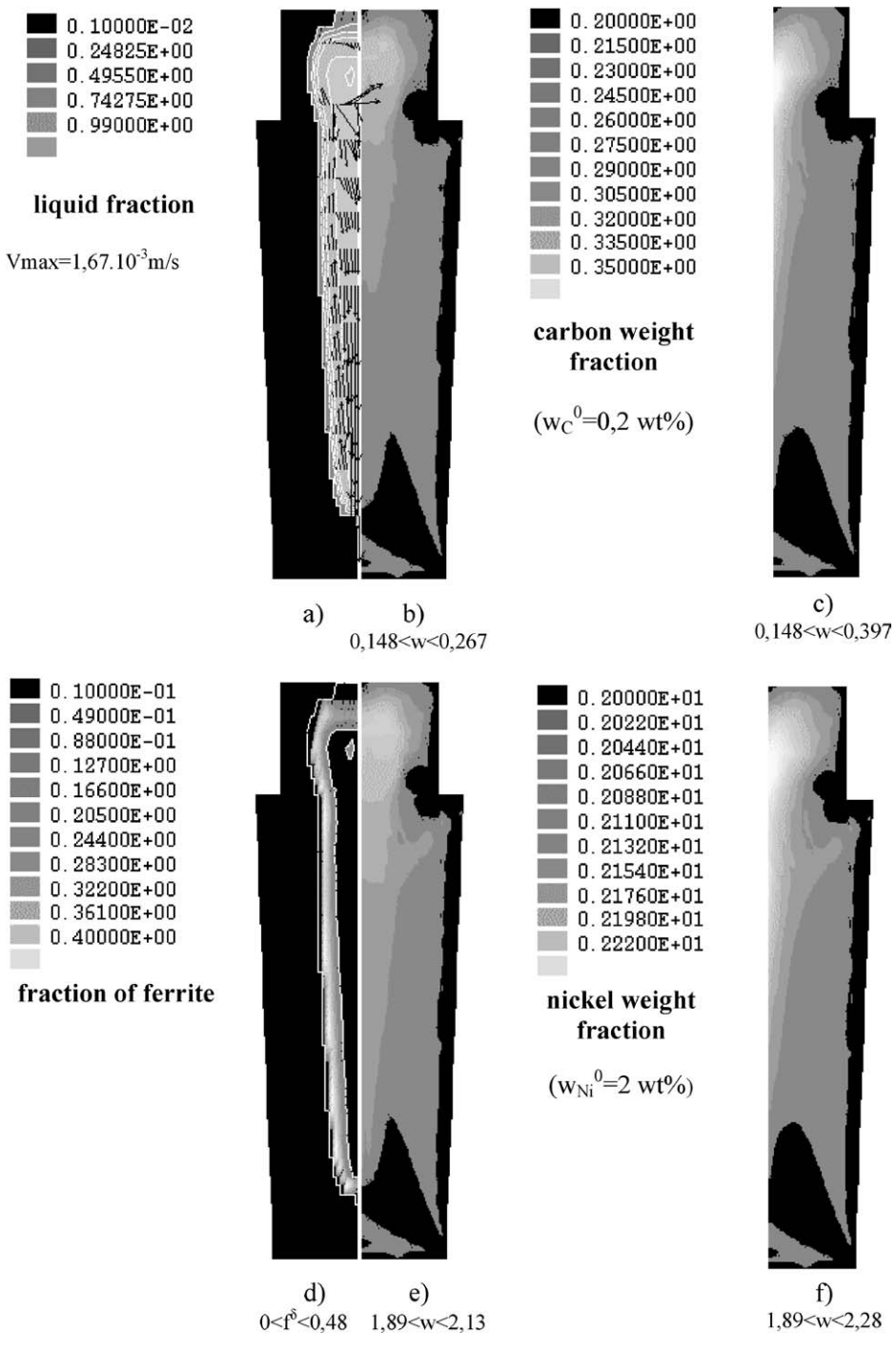

Figure 4 Macrosegregation patterns of carbon (b) at 3428 s, (c) at the end of solidification and macrosegregation patterns of nickel (e) at 3428 s, (f) at the end of solidification. (a) Velocity vectors and liquid fraction at 3428 s. (d) Fraction of ferrite at 3428 s. The white lines delimit the mushy zone.

velocity field represented in Fig. 4a: an upward flow develops in the mushy zone, whereas a downward flow can be observed in the liquid. As a consequence, the enriched liquid in carbon and nickel of the mushy zone goes upwards, which induces a positive macrosegregation in the top part of the ingot and an impoverishment in solute in the bottom part of the ingot (Fig. b, c, e and f). The strongly segregated liquid in the top part of the ingot brings the local solidification path closer to the monovariant line. So, the global amount of ferrite deposed in the mushy zone is lower in the top part of the ingot, as shown in Fig. 4d.

The extent of the positive and negative macrosegregated zones are similar for carbon and nickel. But quantitatively, macrosegregation is more severe for carbon than for nickel. This result is coherent with the fact that the intensity of macrosegregation of an element depends on its partition coefficient. Indeed, the thermodynamic values calculated by Thermo-Calc during solidification show that $k_c^{\delta/l} < k_{Ni}^{\delta/l} < 1$ and $k_c^{\gamma/l} < k_{Ni}^{\gamma/l} < 1$.

The same micro-macro calculation as the previous one has been made, but without taking into account the addition of nickel, i.e., for the binary alloy Fe-0.2 wt%C. Qualitatively, this calculation gives the same final macrosegregation patterns as the previous one for carbon. But, quantitatively, some differences can be observed, as shown in Fig. 6: the positive

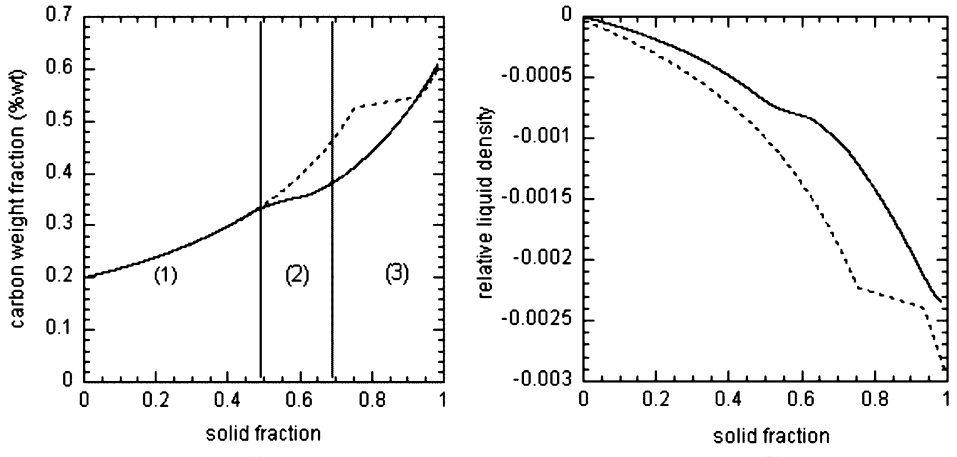

Figure 5 (a) Evolution of carbon content in the liquid at the liquid/solid interface during solidification predicted by the microsegregation model by taking into account the addition of nickel (continuous line) or not (dotted line). (b) Evolution of the relative liquid density in the mushy zone for the solidification path obtained by taking into account the addition of nickel (continuous line) or not (dotted line).

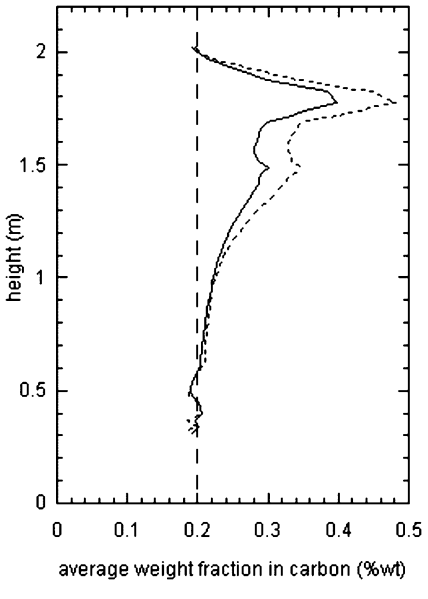

Figure 6 Macrosegregation variation of carbon along the vertical centerline of the ingot at the end of solidification obtained in the ternary case (continuous line) and in the binary case (dotted line).

macrosegregation in carbon along the centerline is less severe in the ternary case than in the binary case.

In order to understand this result, the same method as above has been applied: the solidification path has been calculated by the microsegregation model with (5) and (6) as input conditions, but in the binary case. Fig. 5a compares the evolution of the carbon weight fraction in the liquid at the solid/liquid interface during solidification predicted by the microsegregation model in the ternary case (continuous line) and in the binary case (dotted line). We can observe that the peritectic transformation reduces the increase of the carbon content in liquid. In reference [17], the carbon weight fraction profile has been represented in each phase δ, γ and liquid during the peritectic transformation for a micro-calculation almost similar to the ternary case. This profile is almost plate in each phase, which is due to the high diffusion coefficients of carbon in liquid but also in solid phases. The large migration of the ferrite/austenite interface during the peritectic transformation consumes a large amount of carbon. So, the same quantity must be supplied by a flux of carbon from liquid to austenite, which results in a reduction of the increase of the carbon content in liquid. As a consequence, the peritectic transformation tends to reduce the gradient of the liquid density in the mushy zone, as shown in Fig. 5b, and so the thermo-solutal convection. For the binary or the ternary case, the solidification path can be divided into the three stages already mentioned above, but the peritectic transformation occurs at different liquid fractions indicated in Table IV.

This discussion allows to determine two reasons to the differences observed in Fig. 6:

- the microsegregation of nickel which influences the liquid density through the quantity $\beta_w^{Ni} + \beta_T m_{Ni}^{l/s}$. Its influence is clearly visible in Fig. 5b for solid fractions lower than 45%.
- The modification of the microsegregation of carbon by the addition of nickel. Indeed, in the ternary case, the peritectic transformation occurs when the liquid fraction is more significant than in the binary case. Consequently, the specific effect of the peritectic transformation on the thermo-solutal convection is more important in the ternary than in the binary case. As mentioned above, this effect tends to reduce the gradient of the liquid density in the mushy zone for the studied alloys. It can be noticed that this effect could be much more important if the nominal compositions were closer to

TABLE IV Remaining liquid fractions at the beginning and at the end of the peritectic transformation for the solidification path calculated in the binary and ternary cases

	Liquid fraction at the beginning of the peritectic transformation (%)	Liquid fraction at the end of the peritectic transformation (%)
Fe-Ni-C	52	31
Fe-C	25	8

the monovariant line, i.e., if the peritectic transformation occurred at solid fractions lower than 20% instead of 50%.

4. Conclusions

A microsegregation model, based on an original algorithm in which the Landau transformation is used to treat the one-dimensional diffusion problem during the primary solidification, but also during the peritectic transformation, has been coupled to a macro model. The resulting micro-macro model is then able to predict macrosegregation induced by the liquid motion with an accurate description of microsegregation. An illustrative application to a 3t3 steel ingot has been presented. The Cpu time for a computation which has found to be about 24 h demonstrates that the numerical model is efficient. The influence of the microsegregation on the macrosegregation has been studied. Notably, the increase of the composition of carbon in the liquid phase during solidification is shown to be reduced by the peritectic transformation. Consequently, the gradient of the liquid density in the mushy zone and so the intensity of the thermo-solutal convection is reduced too. The more the peritectic transformation occurs at high liquid fractions, the more this phenomenon is important. This is the reason why it is essential to know when the transformation occurs during the solidification, which is greatly influenced by the amount of nickel present in the studied alloys.

Acknowledgements

This work is sponsored by the research program OSC, which is co-financed by the French research ministry and eight industrial partners (AUBERT&DUVAL, Ascometal, USINOR INDUSTEEL, CTIF, ERASTEEL, PSA, Fonderie de l'Atlantique, S&CC, TRANSVALOR).

References

1. C. BECKERMANN, *Intern. Mater. Rev.* **47**(5) (2002) 243.
2. H. COMBEAU, J.-M. DREZET, A. MO and M. RAPPAZ, *Metall. Mater. Trans.* **27A** (1996) 1314.
3. C. Y. WANG and C. BECKERMANN, *Mater. Sci. Eng.* **171** (1993) 199.
4. M. C. SCHNEIDER and C. BECKERMANN, *Metall. Mater. Trans.* A **26A** (1995) 2373.
5. J. MIETTINEN, *Metall. Trans. A* **23A** (1992) 1155.
6. M. C. SCHNEIDER, J. P. GU, C. BECKERMANN, W. J. BOETTINGER and U. R. KATTNER, *Metall. Mater. Trans.* A **28A** (1997) 1517.
7. J. P. GU and C. BECKERMANN, *ibid.* **30A** (1999) 1357.
8. Y. UESHIMA, S. MIZOGUCHI, T. MATSUMIYA and H. KAJIOKA, *Metall. Trans.* B **17B** (1986) 845.
9. H. W. KERR and W. KURZ, *Intern. Mater. Rev.* **41**(4) (1996) 129.
10. G. BLANC and R. TRICOT, *Mem. Sci. Rev. Met.* **68** (1971) 735.
11. A. A. HOWE, *Micro-Segregation in Multicomponent Steels Involving the Peritectic Reaction*, Ph.D. thesis, Sheffield University, 1993.
12. D. H. ST. JOHN and L. M. HOGAN, *Acta Metall.* **25** (1977) 77.
13. H. FREDRIKSSON and J. STJERNDAHL, *Metall. Trans.* **8A** (1977) 1107.
14. H. FREDRIKSSON, *Metal Sci.* (1976) 77.
15. H. FREDRIKSSON and J. STERNJDAHL, *ibid.* **16** (1982) 575.
16. M. C. SCHNEIDER and C. BECKERMANN, *ISIJ Intern.* **35**(6) (1995) 665.
17. L. THUINET, G. LESOULT and H. COMBEAU, in Liq. Met. Proc. & Casting Conf. 2003, Nancy, Sept. 21–24, edited by Peter D. Lee, Alec Mitchell, Jean-Pierre Bellot and Alain Jardy, 2003, p. 163.
18. N. AHMAD, H. COMBEAU, J. L. DESBIOLLES, T. JALANTI, G. LESOULT, J. RAPPAZ, M. RAPPAZ and C. STOMP, *Metall. Mater. Trans.* A **29A** (1998) 617.
19. X. TONG and C. BECKERMANN, *J. Cryst. Growth* **187** (1998) 289.
20. H. D. BRODY and M. C. FLEMINGS, *Trans. AIME* **236** (1966) 615.
21. T. W. CLYNE and W. KURZ, *Metall. Trans.*, **12A** (1981) 965.
22. X. DORÉ, H. COMBEAU and M. RAPPAZ, *Acta Materiala* **48** (2000) 3951.
23. *Guide to the Solidification of Steels*, Stockholm, Jernkontoret, 1977.

Received 17 March
and accepted 21 June 2004